Observation of Superradiant Amplification of Ultrashort Laser Pulses in a Plasma

M. Dreher, E. Takahashi,* J. Meyer-ter-Vehn, and K.-J. Witte[1]
[1]*Max-Planck-Institut für Quantenoptik, D-85748 Garching, Germany*
(Received 12 December 2003; published 25 August 2004)

We demonstrate the amplification of a femtosecond signal pulse in an underdense plasma by a novel mechanism called superradiant amplification. The pulse is amplified by a counterpropagating few picosecond long pump pulse. In the superradiant regime, the ponderomotive forces exceed the electrostatic forces and arrange the plasma electrons to reflect the pump light into the signal pulse. We found a significant amplification in energy and intensity. The time structure of the amplified signal pulse carries intrinsic features of the superradiant regime. Sub-10-fs pulses of petawatt power appear feasible.

DOI: 10.1103/PhysRevLett.93.095001 PACS numbers: 52.35.Mw, 42.65.Re

The recent years have witnessed significant progress in increasing the peak powers of laser pulses up to the petawatt (PW) level [1,2] by perfecting the chirped-pulse amplification (CPA) technique [3]. Such pulses are indispensible for particle acceleration in plasma [4,5], high-harmonic generation [6], and x-ray lasers [7]. The minimal pulse duration is limited by the gain bandwidth of the amplifying medium. The presently broadest medium is Ti:sapphire yielding 28-fs pulses of PW power [1]. An alternative is optical parametric amplification. It provides larger amplification bandwidths enabling sub-10-fs pulses at currently the μJ level [8]. Its potential for high-energy amplification has yet to be proven.

Two plasma-based amplification schemes have been proposed recently able to directly amplify fs-laser pulses without stretching and recompression. Plasma acting as an amplifying medium can sustain almost arbitrarily high intensities without suffering damages. In both schemes, a short input signal pulse collides with a long counterpropagating pump pulse of slightly higher frequency in an underdense plasma. The electron density is modulated in the interaction region such that the electrons scatter pump light back into the signal pulse. The schemes differ in the way the electrons are arranged.

In this Letter, we experimentally demonstrate for the first time superradiant amplification (SRA) [9] that efficiently amplifies ultrashort pulses and simultaneously increases their bandwidth thereby leading to significant pulse shortening. In the SRA regime, the intensities of the pump and signal pulses are so strong that their common ponderomotive force exceeds the electrostatic forces due to charge separation. Hence the electrons perform forced oscillations at the frequency dictated by the ponderomotive potential. The term SRA implies that all participating plasma electrons coherently backscatter the pump pulse. SRA can amplify a signal pulse close to relativistic intensities at flux levels of several kJ/cm^2. PW pulses with durations of two laser cycles can be obtained within a cross section of less than 1 mm^2.

The second plasma amplification scheme [10,11] is based on stimulated Raman backscattering (SRBS). Pump and signal pulses resonantly excite a plasma wave, which backscatters the pump pulse. The signal pulse is shortened only if the pump pulse is depleted. In general, SRA allows shorter pulse durations than SRBS.

The SRA dynamics can be described in terms of an ensemble of electrons. The motion of an individual electron is governed only by its initial conditions and the ponderomotive potential, while the electron-electron interactions are negligible. As the frequencies of the pump and signal pulses differ only slightly, the phase velocity of their interference pattern is small and most plasma electrons get trapped in the periodic structure of the ponderomotive potential (Fig. 1). The trapped electrons start oscillating with the bouncing frequency $\omega_b^2 = 4a_{pu}a_s\omega_{pu}\omega_s$ [9], where $a_{pu/s} = eA_{pu/s}/(m_e c)$ are the normalized vector potentials of the pump and signal pulses and $\omega_{pu/s}$ their frequencies, respectively. The initially uniformly distributed electrons are periodically bunched and unbunched. This results in narrow density peaks that appear in turn on the two edges of the confining potential wells. The first bunching after a quarter oscillation period leads to the scattering of pump light into the signal pulse. Because of the ongoing oscillation, the density peak decays and the reflection of the pump ceases. When the peak reappears half an oscillation period later on the opposite side of the potential well, the signal pulse is reflected back into the pump pulse and is thereby attenuated.

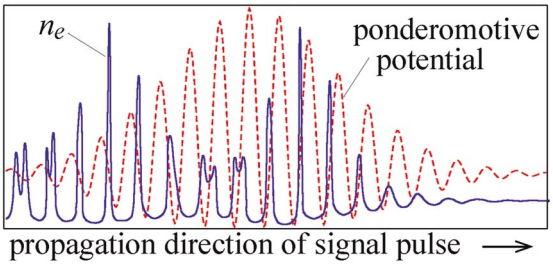

FIG. 1 (color). Snapshot of the electron density n_e in the ponderomotive potential. Potential wells from right to left indicate the evolution of the electron density grating.

 0031-9007/04/93(9)/095001(4)$22.50

Thus an initially short signal pulse is amplified on its leading edge while the attenuation on its rear edge restricts its duration to about one-half of an oscillation period, π/ω_b. Since ω_b increases as the signal amplitude grows, the pulse becomes shorter during the amplification. The coherent scattering follows from the almost perfect bunching of the electrons to layers much thinner than the laser wavelength in combination with the spatial periodicity of the potential. The threshold for the transition from SRBS to SRA is given by $\omega_b > \omega_{pe}$ [9] and sets a lower limit for the intensities of the laser pulses. Here, $\omega_{pe}^2 = e^2 n_e/(\epsilon_0 m_e)$ is the electron plasma frequency.

The Advanced Ti:S Laser (ATLAS) at the Max-Planck-Institute for Quantum Optics provides 200-mJ, 793-nm pulses at 10 Hz. To serve as pump pulses for our experiments (Fig. 2), they are not compressed to the bandwidth limit of 120 fs but only to a few ps by imparting them a negative chirp. The input signal pulse is generated from a small fraction split off from the fully stretched ATLAS pulse. It is separately compressed to 120 fs and broadened to a spectral a range from 740 to 830 nm by self-phase modulation in an Ar-filled hollow fiber [12]. The fiber also filters the pulse spatially, yielding a Gaussian-like intensity distribution with a diffraction-limited beam quality ($M^2 \approx 1$). A dielectric filter blocks the wavelengths below 800 nm, thereby shifting the central wavelength to 815 nm. The nonlinear chirp of the filtered pulse prevents compression to the bandwidth-limited duration of 56 fs corresponding to its 17-nm bandwidth. The compressed pulse has an energy of 70 μJ, a duration of 80 fs (FWHM), and a negatively chirped pedestal that extends to about 170 fs at an intensity level of a few percent of the peak intensity.

In the target chamber, the pump and signal pulses are focused from opposite directions into a H_2 gas jet by off-axis parabolic mirrors of equal focal length. The diameters of the central focal disks extending to the first diffraction minimum are 30 and 26 μm, respectively. Any stray light outside these disks is so weak that it is negligible for the amplification process. About 70% of the pump pulse energy and 85% of the signal pulse energy is contained in the disks. In the focus, the initial intensities are $I_s = 1.3 \times 10^{14}$ W/cm^2 and $I_p = 5.7 \times 10^{15}$ W/cm^2 for a duration of $\tau_{pu} = 3.5$ ps. The Rayleigh length is ≈ 600 μm and lies within the gas jet of 1-mm length. The spatial overlap of the two pulses in the plasma is established by making both pass through a pinhole. Their arrival times are synchronized by means of a streak camera measuring the time lag between them. The delay between both pulses is fine-tuned by optimizing the gain during the experiment.

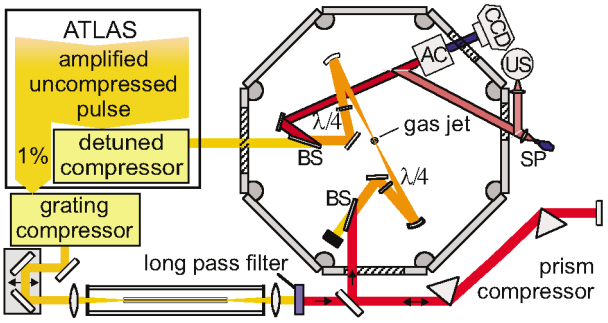

FIG. 2 (color). Experimental setup: BS: polarizing beam splitter; $\lambda/4$: quarter wave plate; AC: single-shot AC; CCD: charge coupled device camera; US: Ulbricht sphere for energy measurement; SP: spectrometer;

As the gas nozzle is closed on the sides except for holes for the pulses, an interferometric measurement of the electron density, n_e, is not possible. Instead n_e is derived from the spectral shift of the Raman backscattered pump light by the relation $n_e = \omega_{pe}^2 \epsilon_0 m_e/e^2$. For the presented experiments, n_e is 3.5×10^{18} cm^{-3} corresponding to 0.002 times the critical density. The ionization blueshift is not relevant for this measurement because the H_2 gas is ionized by the low-intensity leading edge of the pump pulse [13], so that the main part of the pulse interacts with a fully ionized plasma.

After the interaction in the plasma, the reflection from the second off-axis parabola recollimates the two pulses. The individual beam paths are separated by a combination of polarizing beam splitters and $\lambda/4$ wave plates. On both beam splitters, the signal pulse is s polarized and the pump pulse p polarized, so that the pump pulse passes through them and the signal pulse is reflected. The first wave plates alter the polarization state of the incoming pulses to circular polarization of opposite helicity as best for the interaction. The passage through the second wave plate restores the original linear polarizations.

The diagnostics to characterize the signal pulse includes the simultaneous measurement of its energy, spectrum, and autocorrelation (AC) by a single-shot, second-order background free autocorrelator (Fig. 2).

Figure 3(a) shows the energy of the amplified signal pulse versus the delay between both pulses. The output energy reaches its maximum when the region where the pulses meet lies completely within the plasma and the Rayleigh length. The maximal energy of ≈ 1 mJ corresponds to a gain of 19 with respect to the input energy contained in the central focal disk. Shot-to-shot fluctuations of the output energy can be explained by fluctuations of the plasma density and of the intensities of both input pulses. They are correlated because the two pulses originate from the same source.

Initially, the threshold condition for SRA, $\omega_b > \omega_{pe}$, is not satisfied; one finds $\omega_b^2/\omega_{pe}^2 = 0.4$. By amplification the ratio increases to 1.75. The amplified signal intensity is computed from the measured output signal energy, the focus diameter, and the temporal profile obtained from

the AC measurement. Thus the interaction starts in the SRBS regime and enters the SRA regime during the amplification. Raman amplification is possible for short pulses even though the resonance condition is not satisfied strictly. The dephasing due to the frequency mismatch $\Delta\omega = \omega_{pu} - \omega_s - \omega_{pe}$ becomes important only for pulses longer than $\pi/\Delta\omega = 90$ fs.

The amplified signal has a background caused predominantly by the Raman instability of the pump pulse. The backscattered light has the same polarization and occupies the same spectral range as the signal pulse and cannot be separated by a beam splitter. It forms an undesired long weak precursor. The Raman instability is strongly suppressed in the region already passed by the signal pulse because the interaction of the two pulses heats the plasma electrons to keV temperatures corresponding to the depth of the ponderomotive potential. The energy level of the backscattered light is measured with the signal pulse blocked. Since the plasma is not heated by the pump-signal interaction, the pump pulse is scattered over the full length of the plasma and this measurable level will be higher than that in the presence of the signal pulse, which is not directly measurable.

The spectra in Fig. 3(b) reveal whether SRBS or SRA dominates the amplification. The spectral broadening from 17 nm (non-bandwidth-limited input pulse) to 29 nm after the amplification is expected for SRA because of the pulse shortening during the amplification. It is much larger than for pure SRBS, which has its Stokes line around 825 nm and a gain bandwidth $\gamma = \sqrt{\omega_{pu}\omega_{pe}}a_{pu} = 0.17\omega_{pe}$ in the weakly coupled regime [14] corresponding to 6 nm. Including the 8-nm bandwidth of the chirped pump pulse, this is still much less than the observed bandwidth. Bandwidth broadening by amplification in the pump-depleted Raman regime [10] can be excluded, because the observed energy transfer from the pump to the signal pulse is too small.

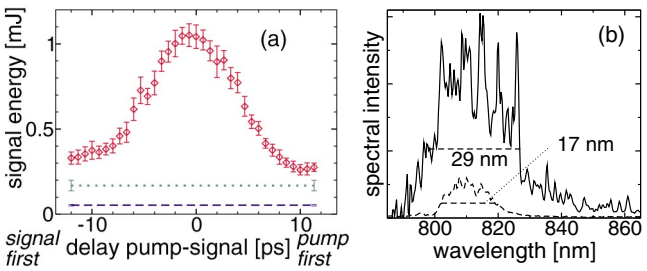

FIG. 3 (color). (a) Energy of the amplified signal vs delay between both pulses (diamonds), input signal energy (dashed line), and backscattered pump light (dotted line) in the absence of the signal pulse. The diamonds represent averages over 30 shots; statistical deviation is indicated by error bars. (b) Input (dashed line) and output (solid line) spectra of the signal pulse for the delay adjusted to maximum amplification.

The 2nd-order AC trace of the amplified signal pulse in Fig. 4 exhibits an oscillating behavior. Apparently, the signal pulse consists of a train of equidistant pulses. The five peaks of the AC trace correspond to three peaks of the amplified signal. Its temporal profile is retrieved by fitting a train of three $\sin^2$ pulses such that its computed AC trace matches the measured trace. The fitted pulses are each 26 fs long and spaced by 54 fs, i.e., each single spike is much shorter than the input pulse.

Although the AC trace is ambiguous as to which pulse leads the train, it is reasonable to assume that the pulse with the largest amplitude comes first, as explained later. The measured energy and known focus diameter yield an intensity of 2.6×10^{15} W/cm^2, about 17 times higher than that of the input pulse. To compute the bouncing frequency ω_b, the pump intensity I_p at the position of the signal pulse is needed. Although I_p changes during the amplification, the uncertainty of the exact value of I_p affects the value of ω_b only slightly because of $\omega_b \sim I_p^{-1/4}$. Assuming $I_p \approx 2 \times 10^{15}$ W/cm^2, which is 35% of the peak value, the calculated pulse duration is $\pi/\omega_b = 28$ fs and the temporal spacing of the succeeding pulses $2\pi/\omega_b = 56$ fs, very close to the measured data.

The breakup into a train of pulses is an intrinsic SRA feature. It appears if the signal pulse is so long that the electrons are trapped for several oscillation cycles in the ponderomotive potential of the signal and pump pulses. The signal pulse is amplified and attenuated periodically and, finally, the periodic attenuation splits it into a train of pulses at regular intervals of one oscillation period, $2\pi/\omega_b$, which is confirmed by the good agreement of the measured and computed durations and temporal distances of the signal pulses.

SRBS cannot cause a regular train of such short pulses. The pump depletion regime exhibiting a pulse train is excluded because of the small energy transfer from the pump to the signal pulse. A beating of a Raman Stokes line with the input signal pulse is ruled out by the absence of two distinct spectral components in the spectrum.

The bunching of the electrons becomes less perfect after several cycles because potential wells are nonhar-

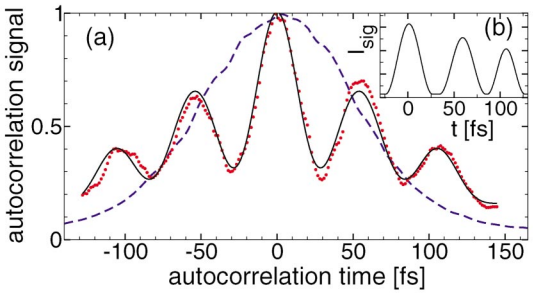

FIG. 4 (color). (a) Normalized AC traces of the input pulse (dashed), amplified output pulse (dots) and fitted signal pulse (solid). (b) Intensity profile of the fitted signal pulse.

monic and thus not all electrons have exactly the same oscillation period. Furthermore, the electrons receive an energy spread of the order of the depth of the ponderomotive potential after the first pulse has passed and cannot be trapped all by the smaller ponderomotive potential of the following pulses. Fewer electrons are bunched and the amplification becomes less efficient. Therefore, the leading pulse is more strongly amplified and finally outgrows the trailing pulses.

The pulse breakup by the amplification in the SRA regime can be reproduced by numerical simulations that we performed with a 1D particle-in-cell (PIC) code. The experimental data are used for n_e and the intensities and durations of the pump and signal pulses. The temporal pulse profiles are taken Gaussian like, the pump pulse is negatively chirped, and the signal pulse has an additional negatively chirped precursor whose intensity amounts to 6% $I_{s,\max}$. The plasma length is 1000 μm with additional 250 μm-long ramps at the edges. The snapshots in Fig. 5 show that the SRA with subsequent pulse breakup sets in only after the signal has been amplified by SRBS. Furthermore, they reveal that the slight lengthening of the pulse train compared to the input pulse is caused by the amplification of the precursor. Although its intensity is very small in the beginning, it can catch up with the main pulse. Plots of n_e and phase space (not shown here) reveal the trapping of a fraction of the electrons when ω_b is still slightly smaller than ω_{pe}, which deteriorates the bunching and thus the amplification when the main pulse passes. Similarly, the signal trailing edge is not significantly built up by SRBS in the Raman regime at the beginning, because the fraction of trapped electrons affect the coherence of the plasma wave behind the signal pulse. In the simulation the energy and intensity amplification are about 2 times larger than those experimentally observed. This is a good agreement considering the idealized 1D plane geometry used in the PIC code.

Finally, the near and far fields of the amplified pulse were examined. The near field shows a smooth, Gaussian-like fluence distribution without hot spots. This indicates that only the central disk of the focus is amplified, where the intensities of both pulses are strongest, as is expected for a good transverse overlap. In the surrounding areas the intensities and hence the amplification is only small. These findings agree with the far-field measurement. The signal pulse was refocused with a lens of long focal length and captured by a CCD camera. Comparing the far-field fluence patterns of the input and amplified signal pulse shows an almost diffraction-limited beam quality of the amplified pulse. Shifting the foci of the pump and signal pulses transversely with respect to each other by a few μm causes interference fringes in the near field pattern, oriented at right angles to the direction of the shift. This sensitivity renders the inspection of the near field a valuable online diagnostic for an exact overlap.

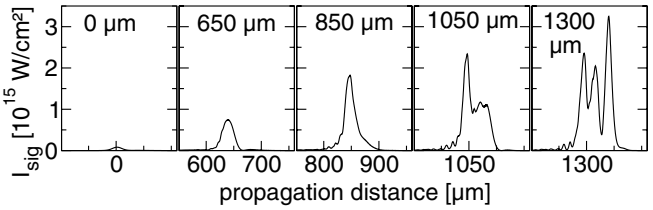

FIG. 5. A PIC simulation in the comoving rest frame illustrating evolution of the signal pulse. Snapshots of the signal intensity are displayed after a propagation distance indicated in the individual plots. The signal pulse travels to the right.

In conclusion, we have demonstrated SRA. This is proven by (i) an amplification of about 20 in energy and intensity, (ii) the breakup of the amplified signal pulse into a sequence of pulses of duration π/ω_b separated by $2\pi/\omega_b$, and (iii) by spectral broadening of the signal pulse. The effect (ii) causes the shortening of the pulse if it has an initial duration $\leq 2\pi/\omega_b$. The good focusability of the amplified signal pulse renders the SRA mechanism attractive as a final amplification stage of a CPA laser system. Furthermore, the results show that a weak input signal pulse is initially amplified in the Raman regime until its intensity becomes sufficiently large to enter the SRA regime. To start directly in the SRA regime, the intensity of the input signal can be increased by using tighter focusing of both pulses. This approach is appropriate for achieving PW powers, because the amplification starts within the short Rayleigh length and proceeds into the diverging beam, thus distributing the energy over an increasing area, and keeping the intensity below the relativistic level.

The authors thank G. Shvets, A. Pukhov, S. Kalmykov, M. Jost, and D. Habs for fruitful discussions. This work was supported by Euratom-IPP and by the DFG, under Contract No. WI1713/2-1.

*Present address: AIST, Tsukuba Ibaraki, 3058568 Japan.

[1] M. Aoyama *et al.*, Opt. Lett. **28**, 1594 (2003).
[2] M. D. Perry, *et al.*, Opt. Lett. **24**, 160 (1999).
[3] D. Strickland and G. Mourou, Opt. Commun. **55**, 447 (1985).
[4] R. A. Snavely *et al.*, Phys. Rev. Lett. **85**, 2945 (2000)
[5] V. Malka *et al.*, Science **298**, 1596 (2002).
[6] P. A. Norreys *et al.*, Phys. Rev. Lett. **76**, 1832 (1996).
[7] T. Kawachi *et al.*, Phys. Rev. A **66**, 033815 (2002)
[8] G. Cerullo *et al.*, Opt. Lett. **23**, 1283 (1998); A. Shirakawa *et al.*, *ibid.* **23**, 1292 (1998).
[9] G. Shvets *et al.*, Phys. Rev. Lett. **81**, 4879 (1998).
[10] V. M. Malkin *et al.*, Phys. Rev. Lett. **82**, 4448 (1999).
[11] Y. Ping *et al.*, Phys. Rev. E **67**, 016401 (2003).
[12] M. Nisoli *et al.*, Appl. Phys. Lett. **68**, 2793 (1996)
[13] A. Scrinzi *et al.*, Phys. Rev. Lett. **83**, 706 (1999).
[14] D.W. Forslund *et al.*, Phys. Fluids **8**, 1002 (1975).